Electron Spin Resonance, Electron Spin Echo Modulation, and Electron Nuclear Double Resonance Studies of the Photoionization of *N*-Alkyl-*N,N',N'*-trimethylbenzidine in Anionic and Cationic Micelles

Chris Stenland and Larry Kevan*

Department of Chemistry, University of Houston, Houston, Texas 77204-5641

Received: December 14, 1992; In Final Form: February 22, 1993

N-Alkyl-*N,N',N'*-trimethylbenzidines (C_nTMB, n = 1–6, 8) were synthesized and photoionized in rapidly frozen anionic and cationic micelles. The photoyields of the cation radicals were investigated by electron spin resonance spectroscopy. Electron spin echo modulation spectroscopy and proton matrix electron nuclear double resonance were used to determine the relative location of the photoproduced cation radical with respect to the deuterated aqueous interface. No dependence on the photoyield as a function of the electron donor alkyl chain length is observed, although increasing the alkyl chain length on the benzidine moiety moves its location toward the aqueous interface. The lack of a photoyield trend is interpreted in terms of the solubilization geometry, which determines the paths of electron escape to form charge-separated products. An electron escape cone defined as the solid angle formed from the center of the electron donor moiety through the width of the spin distribution that intersects the interface changes only slowly as a function of radical location over a limited range. Hence, the photoyield is little changed.

Introduction

There is considerable interest in studying the photoionization of electron donors with low ionization potentials in micellar solutions.[1-3] An important question is, what are the structural features that determine the optimum net photoyield?[4] Micelles offer an easily modifiable model system that allows investigation into several aspects of charge separation across a lipid interface. There are at least two basic strategies to study the structural features which control the net photoyield in micelles. The first is to alter the micelle. This can be done by changing the size and charge of the micelle by varying the alkyl chain length of the surfactant and the charge of the head group. Next, the micellar interface is modified by adding counterions,[5] cosurfactants,[6] alcohols,[7] and electron acceptors.[8] Another strategy is to alter the electron donor by adding alkyl chains of different lengths to the electron-donor moiety in order to control the solubilization location within the lipid membrane. This location control of electron donors has been demonstrated in several organized molecular assemblies.[9-13]

The one-photon photoionization process of *N,N,N',N'*-tetramethylbenzidine (TMB) in aqueous micellar solutions has been extensively studied.[14-20] This work extends studies of the photoionization of TMB in micelles. Here the benzidine moiety is functionalized at an *N*-alkyl position, forming the class of neutral asymmetric molecules *N*-alkyl-*N,N',N'*-trimethylbenzidines (C_nTMB), also called alkylbenzidines in this paper. The added alkyl chains range in length from C_2 to C_8. The synthesis and ESR parameters of these compounds have not been published before. Continuous-wave electron spin resonance (ESR) is used for the both the identification and determination of the net yield of photogenerated radicals. Electron spin echo modulation (ESEM) spectroscopy and proton matrix electron nuclear double resonance (ENDOR) have proven to be well suited to investigation of the local nuclear environment around the photoproduced radicals in microheterogeneous media. When D_2O is used in place of H_2O, both ESEM and ENDOR can be used to determine changes in the relative positions of the membrane-solubilized radical to the deuterated aqueous interface as a function of alkyl chain length on the photoionizable molecule.

Experimental Section

Synthesis. The synthesis of *N*-alkyl-*N,N',N'*-trimethylbenzidines is accomplished in three steps. The first step is a molten metal salt reaction that oxidatively couples a mixture of *N*-methylaniline and *N,N*-dimethylaniline to form a mixture of benzidine products. Then by careful flash column chromatography, the *N,N,N'*-trimethylbenzidine is isolated. Step two reacts the trimethylbenzidine with either an acid chloride or anhydride, yielding the trimethylbenzidine amide. The final step is the reduction of the amide to the tertiary amine, which is again purified by flash column chromatography.

***N,N,N'*-Trimethylbenzidine.** The technique to synthesize *N,N,N'*-trimethylbenzidine follows a literature procedure.[21] The quantities 29.8 g of KCl (Mallinckrodt, reagent grade), 23.4 g of NaCl (Mallinckrodt, reagent grade), and 160 g of $AlCl_3$ (Aldrich, anhydrous 98%) were added to a 1-L two-necked round-bottom flask containing a 1-in. egg-shaped Teflon-coated magnetic stir bar. The salts were anhydrous and used as received. The flask was lightly capped and placed into a silicon oil bath preheated to 150 °C. After about 30 min, the salt mixture had melted to form a dark low-viscosity liquid which was easily stirred with a magnetic stir bar. A condenser was fit on the flask, and a gas inlet adapter which carried O_2 gas is also fitted. The oxygen gas inlet tube is adjusted so it is within 1.0 cm above the molten salt. Then a mixture of 0.0549 mol of *N*-methylaniline (Aldrich, 99%) and 0.0549 mol of *N,N*-dimethylaniline (Aldrich, 99%) was added to the mixture through the condenser. The mixture evolves HCl gas, and the flask above the salt mixture becomes metallic red with streaks of yellow and green. Once the anilines are added, the O_2 is blown over the mixture at a rate of 20 mL/min.

After 10 h, the oxygen gas flow is stopped and the molten salt mixture is removed from the bath, the excess oil is allowed to momentarily drain, the bottom is wiped with a paper towel, and the molten salt is quickly, but carefully, poured into a 2-L Erlenmeyer flask containing 1 L of 0.1 M HCl with crushed ice in an ice bath. (**Warning**: HCl gas is evolved in large quantity.) The round-bottom flask, condenser, and gas tube are rinsed with deionized water into the quenching solution. The Erlenmeyer flask is then removed from the ice bath and sits overnight. The solution is filtered and then neutralized with concentrated NaOH

0022-3654/93/2097-5177$04.00/0

(Baker, reagent grade), and the aqueous phase is exhaustively extracted with diethyl ether (EM Scientific). The ether is removed under vacuum with a rotary evaporator. The resulting material is a somewhat mobile, tarry material. Thin-layer chromatography (TLC) on silica gel, Whatman PE SilG/UV, with benzene:acetone 80:20 (v:v) (benzene and acetone are Mallinckrodt reagent grade stored over a 4-Å molecular sieve to remove trace water) shows the presence of three primary benzidines (TMB, *N,N,N'*-trimethylbenzidine, and *N,N'*-dimethylbenzidine) and at least two other benzidines (possibly chlorobenzidines[21]) as minor products plus other unknown products with small R_f values after exposure to I_2 vapor. Under ultraviolet light, the starting materials are also visible. The starting materials are removed by steam distillation followed by extraction into methylene chloride (Mallinckrodt, reagent grade), drying over $MgSO_4$ (Mallinckrodt, anhydrous reagent grade), and removal of methylene chloride in a rotary evaporator. The crude material is dissolved in a minimum of benzene:acetone 80:20 (v:v) and passed through 4 in. of silica gel, 60–200 mesh (Mallinckrodt, SilicAR grade 62) on a 3-in.-diameter column. The benzidines are eluted with the benzene:acetone 80:20 (v:v) solution. The solution is still dark, but after evaporation of the solution some yellow crystals are visible. The benzidine products come over quickly, and dark colored material continued to be eluted long after the benzidines passed through. Typically the first 500 mL or less of elutant contains nearly all the benzidines.

The next step is the isolation of *N,N,N'*-trimethylbenzidine. Seven inches of silica gel for flash chromatography (Aldrich, 200–400 mesh, 60 Å) is wet packed on a 2.5-in. column. The mobile phase is 20:1 benzene:acetone with one drop of triethylamine (Fisher, reagent grade). The benzidines are dissolved in a minimum of eluting solution, and to this solution is added one drop of triethylamine. The benzidines are carefully added, then drawn into the silica, and allowed to sit for 5 min, during which time the column is filled with the eluting solvent. The column is sealed, and 5–8 psi of pressure from a nitrogen tank is used to force the solution through the column. Fractions of 10–50 mL are collected until no more benzidines are detected by TLC.

By repeating the flash chromatography using fresh silica gel and selecting the fractions that contain mostly *N,N,N'*-trimethylbenzidine, the other two major benzidine products are depleted, yielding after three or four cycles nearly pure trimethylbenzidine.

This measure of purification for trimethylbenzidine is needed for the production of *N*-ethyl-, *N*-propyl-, and *N*-butyl-*N,N',N'*-trimethylbenzidine since later isolation from residual TMB, if not removed beforehand, is very difficult even with flash chromatography. For *N*-alkyl chains longer than C_4, the final product can be isolated from small amounts of the TMB and the *N,N'*-dialkyldimethylbenzidine products.

N,N',N'-Trimethylbenzidine Amide. Trimethylbenzidine is reacted with an equimolar amount of an acid chloride or anhydride by refluxing in benzene for 24 h (acetic anhydride, Baker, 98.9%; propionic anhydride, 97%; butyric anhydride, 98%; valeric anhydride, 99%; hexanoic anhydride, 99%; octanoyl chloride, 99%; decanoyl chloride, 98%; lauroyl chloride, 98%; and palmitoyl chloride, 98%, Aldrich). After cooling, the benzene solution is washed with water and then with dilute NaOH solution until the excess acids have been removed. Finally the solution is washed with water again. The solution is dried with $MgSO_4$ overnight and filtered, and the benzene is evaporated under reduced pressure in a rotary evaporator.

***N*-Alkyl-*N,N',N'*-trimethylbenzidine.** The amide is placed into a Soxhlet thimble and extracted into a refluxing solution of an excess of lithium aluminum hydride (Aldrich, 95%) in anhydrous ether. The refluxing of the solution continues for 2 days, after which time the extractor is replaced with a water-cooled condenser and a round-bottom flask containing the ether solution is packed on an ice bath. After the solution is chilled, small chips of ice are added followed by small amounts of water until the gray ether solution turns lighter, indicating that enough water has been added to the solution. The solution is stirred for several hours to give a white solution of aluminum hydroxides, indicating total hydrolysis of the reduction mixture. The solution is filtered, and the white cake is washed with much ether. The ether solution is dried using a salt-saturated, deionized water solution. The ether filtrate is typically light yellow to colorless and is evaporated under reduced pressure in a rotary evaporator, leaving a light-yellow oil which crystallized to a light colored material. This material is dissolved into a minimum amount of benzene plus one drop of triethylamine and purified by flash chromatography on 45 cm of silica gel in a 1.5-in.-diameter column. The elutant for C_1TMB through C_4TMB is 20:1 benzene:acetone, while for C_5-TMB through C_{16}TMB the elutant is pure benzene. Typical volumes of the fractions collected are 20 mL. Pure fractions of the C_nTMB, as determined by analytical TLC (Whatman MK6F, silica gel), are collected, and the solvent is evaporated, leaving a colorless solid.

The products' identity is confirmed by ^{1}H and proton-decoupled ^{13}C NMR on a GE QE-300 NMR spectrometer and by mass spectroscopy, which was performed on a VG-70-SEQ-300 mass spectrometer where the ions were produced by fast atom bombardment (8 keV Xe^+) in a matrix of *m*-nitrobenzyl alcohol. The alkylbenzidines were also investigated optically on a Perkin-Elmer 330 spectrophotometer. Optical spectra were compared (vide infra) to commercial sources of *N,N,N',N'*-tetramethylbenzidine (Aldrich and Kodak) purified in the same manner as the synthesized products.

Summary of MS and NMR Data. The *m/e* of the parent ion is listed, followed by the expected mass based on the molecular formula and the masses of the most abundant nuclei where ^{12}C is 12.000. All ^{1}H and proton-decoupled ^{13}C were recorded using $CDCl_3$ as the solvent. TMS was used as an internal standard. The ^{1}H integrals were evaluated by comparing the integral of aromatic protons to the integral of the alkyl protons, denoted here as "Arom/Alkyl". The molecular formula gives the expected ratio of aromatic to alkyl protons, and it is listed for comparison. Finally, the ^{1}H peaks were assigned. The ^{13}C NMR data are listed in ppm. No independent experimental evidence was acquired to assign each peak to a specific carbon atom. Instead, the peaks are listed broadly in terms of belonging to the alkyl and aromatic portions of a C_nTMB molecule.

C_1TMB: Mass 240.0, expected 240.14. Arom/alkyl protons = 0.67, expected 0.67. ^{1}H: δ 3.0, singlet (–N–CH_3); δ 6.6–7.8, aromatic protons. ^{13}C: alkyl 40.9; aromatic 113.59, 127.09, 130.42, 150.

C_2TMB: Mass 254.28, expected 254.16. Arom/alkyl protons = 0.56, expected 0.57. ^{1}H: δ 3.0, singlet (–N–CH_3); δ 3.45, quartet, J = 6.93 Hz (–N–CH_2–C); δ 1.15, triplet, J = 7.5 Hz (*n*-C–CH_3); δ 6.6–7.8, aromatic protons. ^{13}C: alkyl 11.8, 38.1, 42.2, 47.5; aromatic 114.6, 127.6, 129.9, 148.4, 150.

C_3TMB: Mass 268.29, expected 268.17. Arom/alkyl protons = 0.51, expected 0.50. ^{1}H: δ 3.0, singlet (–N–CH_3); δ 3.34, triplet, J = 7.16 Hz (–NCH_2–C–C); δ 1.68, sextet, J = 7.45 Hz (N–C–CH_2–C); δ 1.15, triplet, J = 7.16 Hz (N–C–C–CH_3); δ 6.6–7.8, aromatic protons. ^{13}C: alkyl 12.17, 20.70, 39.1, 41.26, 55.31; aromatic 113.03, 113.64, 127.41, 127.53, 129.61, 130.51, 148.5, 150.

C_4TMB: Mass 282.28, expected 282.18. Arom/alkyl protons = 0.45, expected 0.44. ^{1}H: δ 3.0, singlet (–N–CH_3); δ 3.31, triplet, J = 7.41 Hz (–N–CH_2–C–C–C); δ 1.55, quintet, J = 7.41 Hz (N–C–CH_2–C–C); δ 1.41, sextet, J = 7.41 Hz (N–C–C–CH_2–C); δ 1.15, triplet, J = 7.41 Hz (N–C–C–C–CH_3); δ 6.6–7.8, aromatic protons. ^{13}C: alkyl 14.81, 21.3, 29.76, 39.15, 41.53, 53.31; aromatic 112.96, 113.56, 127.38, 127.41, 129.36, 131.08, 148.67, 150.0.

C_5TMB: Mass 297.0, expected 296.20. Arom/alkyl protons = 0.39, expected 0.40. ^{1}H: δ 3.0, singlet (–N–CH_3); δ 3.31, triplet, J = 7.41 Hz (–N–CH_2–C–C–C–C); δ 1.55, quintet, J = 7.41 Hz (N–C–CH_2–C–C–C); δ 1.41 methylene multiplet envelope, J = 7.41 Hz (N–C–C–CH_2–CH_2–C); δ 1.10, triplet, J = 7.41 Hz (N–C–C–C–C–CH_3); δ 6.6 to 7.8, aromatic protons. ^{13}C: alkyl 14.79, 23.07, 26.92, 29.99, 38.87, 41.43, 53.34; aromatic 112.98, 113.65, 127.35, 127.72, 129.68, 131.73, 148.66, 150.0.

C_6TMB: Mass 311.0, expected 310.21. Arom/alkyl protons = 0.35, expected 0.36. ^{1}H: δ 2.95, singlet (–N–CH_3); δ 3.31, triplet, J = 7.41 Hz (–N–CH_2–C–C–C–C–C); δ 1.58, multiplet, J = 7.41 Hz (N–C–CH_2–C–C–C–C); δ 1.41, methylene multiplet envelope, J = 7.41 Hz (N–C–C–CH_2–CH_2–C); δ 1.10, triplet, J = 7.41 Hz (N–C–C–C–C–CH_3); δ 6.6–7.8, aromatic protons. ^{13}C: alkyl 14.30, 23.0, 26.77, 29.98, 31.90, 38.50, 40.81, 53.18; aromatic 112.41, 113.25, 126.97, 127.29, 129.18, 131.95, 148.20, 149.51.

C_8TMB: Mass 339.0, expected 338.24. Arom/alkyl protons = 0.31, expected 0.30. ^{1}H: δ 1.0–1.8, methylene envelope; δ 3.0–3.6, methyl protons; δ 6.6–7.8, aromatic protons. ^{13}C: alkyl 14.60, 23.21, 27.14, 27.77, 29.62, 30.20, 32.55, 38.81, 41.07, 53.45; aromatic 112.94, 113.52, 127.41, 127.19, 129.58, 130.66, 148.66, 150.0.

Surfactants. Sodium decyl sulfate ($C_{10}SO_4Na$), sodium dodecyl sulfate ($C_{12}SO_4Na$), and sodium tetradecyl sulfate ($C_{14}SO_4Na$) were obtained from Eastman Kodak. These surfactants were recrystallized from ethanol:water 95:5 (ethanol from Midwest Grain Products Co). The water was deionized with a Millipore system giving 18 mΩ cm resistivity. These surfactants were crystallized, washed with diethyl ether, dried in an air stream, and stored under vacuum.

Dodecyltrimethylammonium chloride ($C_{12}N(CH_3Cl)$), tetradecyltrimethylammonium chloride ($C_{14}N(CH_3)_3Cl$), and hexadecyltrimethylammonium chloride ($C_{16}N(CH_3)_3Cl$) were purchased from Eastman Kodak. These hygroscopic cationic surfactants were recrystallized from acetone, washed with diethyl ether, and quickly stored under vacuum several days to remove the residual solvent.

All glassware and magnetic stir bars were solvent washed (H_2O, alcohol, chloroform, alcohol, H_2O) and baked dry. Glassware was stored in aluminum foil until used to keep it free of dust.

Stock Solutions. Stock solutions of surfactants of 0.1 and 0.2 M were prepared in deoxygenated (bubbling dry nitrogen gas for 5 min) deuterium oxide (Cambridge Isotope Labs).

Stock solutions of the C_nTMB compounds were prepared in chloroform, and their concentrations were determined optically with a Varian Techtron Model 635 spectrophotometer. From the optical data, volumes of solution needed to make 4×10^{-4} M for 1-mL volumes were added to test tubes, and a thin film was made by removing the chloroform by a stream of nitrogen gas blown over the surface. After all the chloroform was removed, the test tube was placed in a desiccator and put under vacuum for several hours to remove the last traces of chloroform. After evacuation, the tubes with the thin films were capped with a square of Parafilm (American Can Co.) and stored in a refrigerator until used. The stock chloroform solutions of the C_nTMB compounds were tightly capped and stored in a freezer.

A 0.01 M stock solution of potassium ferricyanide (Aldrich, 99%) was prepared in H_2O to be used in the chemical oxidation of the C_nTMB compounds in $C_{12}SO_4Na$ micelles.

Micelle Sample Solutions. To the C_nTMB thin films was added 1 mL of surfactant solution along with a flea stir bar, and the test tubes were tightly capped with Parafilm. The samples were heated (typically 10–20 deg above the Krafft temperature of the surfactant) for at least 3 days in subdued light to give clear solutions. The C_nTMB concentration was determined by optical spectroscopy. The extinction coefficients for all the C_nTMB compounds was 3.4×10^4 M^{-1} cm^{-1}.[22] The sample chamber on the Varian Techtron spectrophotometer was thermostated to allow measurement of micellar solutions with Krafft temperatures above room temperature.

The micelle solutions (50 μL) containing C_nTMB were added to 2-mm-i.d. × 3-mm-o.d. Suprasil quartz tubes (Hereaus Amersil) flame sealed at one end. (These tubes near the open end were tied with thread in order to place and retrieve the tubes in the liquid nitrogen and helium baths. The thread had a label attached at the other end which identified the tube and stored the excess length of the thread when not in use.) The tube then was sealed at the other end with Parafilm and allowed to equilibrate in a bath above the Krafft temperature in the tube for 1 h. After 1 h, the Parafilm was removed and the sample was plunged into liquid nitrogen to rapidly freeze the sample. The sample was stored under liquid nitrogen throughout the experiments.

To study the solution state ESR, the C_nTMB compounds were prepared as above in micellar solutions in H_2O. The potassium ferricyanide stock solution (10 μL) was added to a 2-mL screw cap sample vial. To this was added 0.400 mL of 0.1 M $C_{12}SO_4Na$ containing C_nTMB. The solution was mixed, immediately turning greenish-yellow, indicating oxidation of the C_nTMB to the cation radical. The solution was then degassed by five freeze–pump–thaw cycles with a nominal vacuum of 100 mTorr. The last cycle was repressurized with dry nitrogen. The vial was removed from the vacuum line and capped. Next, 50-μL pipets (Curtin Matheson) were purged with dry nitrogen gas, and a C_nTMB micelle solution with ferricyanide was drawn into the pipets. The pipets were then flame sealed at both ends. The exterior of the pipet was washed, and the ESR was immediately measured.

Photoirradiation. Photoirradiation was carried out at 77 K in a quartz finger Dewar containing liquid nitrogen. The finger Dewar was rotated approximately 4 times per minute to uniformly irradiate the sample. The light source was a Cermax ILC Technologies 300-W UV-enhanced xenon arc lamp (ILC-LX 300 UV). This lamp was energized by an ILC Technology Model PS300-1 power supply operating at a lamp current of 10 A. The light was filtered through a 10-cm water filter and a Corning 7-60 UV band-pass filter with transmittance in the range 300–400 nm with a maximal transmittance of 70% at 365 nm. Typical light flux intensity at the sample was 140 W m^{-2} (YSI Kettering Model 65 radiometer). The time of irradiation was controlled by a lab-built shutter, activated by a Lucas Ledex rotary solenoid controlled by a Gralab 605 timer.

Magnetic Resonance. ESR spectra were acquired on a Bruker ESP 300 X-band spectrometer with 100-kHz Zeeman field modulation with 1.1-G (uncorrected) modulation amplitude. The incident microwave power was 2.0 mW. The samples were measured at 77 K in a quartz finger Dewar filled with liquid nitrogen. The photoyields were determined by doubly integrating the first derivative absorption spectra using the ESP 300 software.

Two-pulse electron spin echo (ESE) signals were obtained on a home-built spin echo spectrometer operating at X-band, with the samples at 4.2 K using 40-ns exciting pulses. The ESE data were transferred to an IBM PC and then analyzed by new software to determine the normalized modulation depth[7] at the first minimum near 0.7 μs.

Proton matrix ENDOR spectra were recorded at 140 K using a Bruker ESP 350 ENDOR unit interfaced to the Bruker ESP 300 spectrometer. The temperature in the ENDOR cavity was controlled by a Bruker ER4111VT nitrogen flow variable-temperature unit. The radio frequency power was FM modulated at 12.5 kHz so that first-derivative spectra were obtained, and the incident microwave power was 2.0 mW. The number of scans varied between 16 and 256 depending on the signal-to-noise quality, though typically good signals were achieved with 64 scans. The proton matrix ENDOR line width was measured as the peak-

to-peak line width of the first-derivative spectra using the Bruker ESP 300 software.

The solution-state ESR samples were thermostated with the Bruker ER4111VT nitrogen flow unit. Typical spectrometer parameters to acquire these room temperature spectra were as follows: microwave power, 6.2 mW; microwave frequency, 9.53 GHz; nominal center field, 3400 G; scan range, 72 G; sweep time, 83.89 s; and filter time constant, 81.92 ms. Typically, 256 or more scans were acquired to realize good signal-to-noise for these room temperature ESR spectra. The software used to simulate the C_nTMB radical spectra was version 1 of EPR Calc supplied with the Bruker ESP 300 software package.

The initial rate of cation radical production as a function of solubilization location was investigated. Duplicate samples of C_nTMB were solubilized at equal concentrations in $C_{12}SO_4Na$ and $C_{14}SO_4Na$ micelles. The samples were irradiated in 5-s intervals for an integrated time of 1 min and then further irradiated for a total of 10 min to compare with a standard experiment. After each irradiation, the ESR signal was recorded.

Results

Identification and Characterization of the C_nTMB Cation Radicals. The rapidly frozen micellar solutions containing the C_nTMB compounds were white polycrystalline solids with no detectable ESR signals before irradiation. All C_nTMB compounds showed a strong green phosphorescence when the photoirradiating ultraviolet light beam was shut off. After irradiation, the polycrystalline matrix was yellow, indicating the presence of a benzidine-type cation radical. ESR showed a broad singlet with a first-derivative line width of 23 G and g-factor of 2.004 for all C_nTMB$^+$, consistent with earlier ESR parameters measured for TMB$^+$ in micelles.[22] The ESR spectra for all C_nTMB$^+$ in frozen polycrystalline micelles were identical to radicals produced from commercially available *N,N,N',N'*-tetramethylbenzidine. The solution-state ESR of C_nTMB$^+$ produced by chemical oxidation with potassium ferricyanide in 0.1 M SDS is shown in Figure 1. The ESR hyperfine pattern changes from C_1TMB to C_3TMB, but no changes in the ESR hyperfine patterns are seen for longer alkyl chain lengths. The hyperfine couplings constants of these asymmetric cation radicals were determined by spectral simulations and are shown in Table I. They agree well with the couplings previously reported for tetramethylbenzidine.[23,24] The optical absorption spectra in the 430–480-nm range of rapidly thawed photoirradiated C_nTMB in 0.1 M $C_{12}SO_4Na$ are identical to that of TMB$^+$ in the same micelles.[17] In methylene chloride solution, the λ_{max} shifts monotonically from 311.2 ± 0.5 nm for C_1TMB to 314.2 ± 0.5 nm for C_{16}TMB. A similar trend was noted in the λ_{max} for alkylmethylviologens.[25]

Electron Donor Alkyl Chain Effect. The net photoyield as measured by continuous-wave ESR for anionic and cationic micelles is shown in Figure 2. This figure shows that the photoyield is essentially constant over the range of alkyl chain lengths for both cationic and anionic micelles with different surfactant chain lengths. Fitting the photoyield data with a straight line shows a slight decrease. This apparent trend is probably due to the difficulty of solubilizing C_8TMB in micelles, to make it in equal concentration to the shorter chained alkylbenzidines. The concentrations of C_8TMB were slightly less (typically 3–8%) than all the other C_nTMB compounds used. After correcting for the difference in concentration (not shown in Figure 2), the net photoyield is about constant within experimental error. The concentration correction required a curve of net photoyield versus [C_8TMB] for a 10-min irradiation time and extrapolation to 3×10^{-4} M C_8TMB. This curve was generally linear for concentrations below 1×10^{-4} M and then leveled off above this concentration. Using micellar alkylbenzidines at concentrations of 3×10^{-4} M put the net photoyield into a region where small concentration differences have a very small effect on the total yield. The difference in concentration of the C_8TMB is due to the rate at which it is solubilized in the micellar solution. Thin films of C_1TMB through C_6TMB were solubilized to 3×10^{-4} M in the micellar solution by stirring at 35 °C for about 8 h, while it would take about 3 days at this temperature to get C_8TMB into this same concentration range. Stirring at higher temperatures increases the rate of solubilization, but radicals are then thermally produced in anionic micelles; consequently, the gentler solubilization conditions were employed. No thermally produced radicals were observed in cationic micelles.

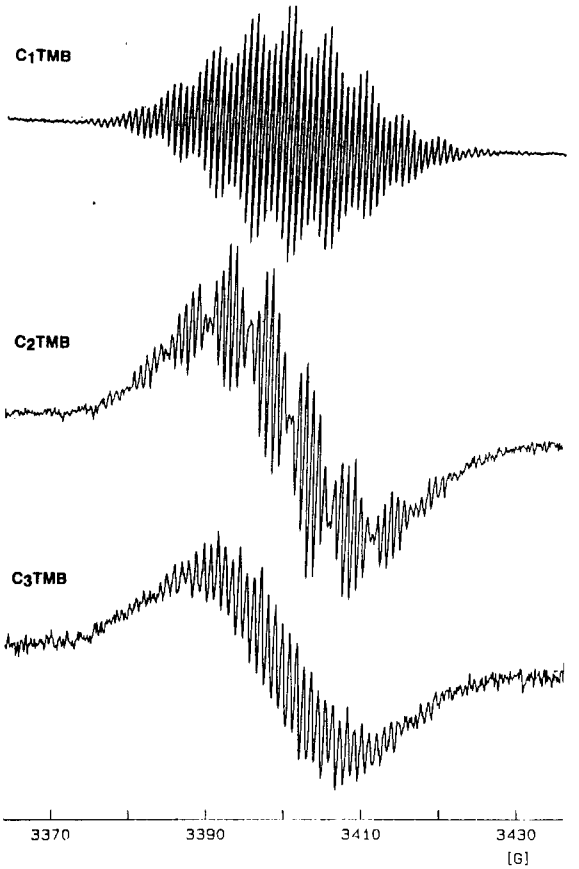

Figure 1. Solution-state ESR obtained by potassium ferricyanide oxidation of C_1TMB (top), C_2TMB (middle), and C_3TMB (bottom) in 0.1 M sodium dodecyl sulfate micelles at 298 K.

Electron spin echo modulation spectroscopy was performed on samples that employed D_2O as the aqueous phase. The echo decay curves exhibited modulations with a period of 0.5 μs, indicating an electron–deuteron interaction. The normalized modulation depth was measured as described in the literature.[7] Figure 3 shows that, for the larger anionic micelles (C_{12}, C_{14}), the normalized modulation depth increases slightly as the alkyl chain length increases. For small anionic micelles (C_{10}), the normalized modulation depth remains constant. A similar trend of increasing normalized modulation depth as a function of increasing alkyl chain length of the alkylbenzidines in cationic micelles is shown in Figure 4.

Proton matrix ENDOR was acquired on the same samples investigated by ESEM. Figures 5 and 6 also show an effect of alkyl chain length on the proton matrix ENDOR line width. In smaller micelles, the ENDOR line width remained constant, while in larger micelles the line width slightly decreased as a function of alkyl chain length.

Effect of Micelle Charge and Size on the Photoyield. The photoyield of C_nTMB$^+$ is greater in frozen cationic micelles than it is in frozen anionic micelles (Figure 2). The difference in yield is approximately a factor of 2–5 depending on the alkyl chain length of the surfactant.

TABLE I: Hyperfine Coupling Constants of *N*-Alkyl-*N*,*N*',*N*'-trimethylbenzidine Cation Radicals in 0.1 M Sodium Dodecyl Sulfate Micelles[a] at 298 K

a_N	a_{CH_3}	$a_{\alpha\text{-}CH_2}$	$a_{\beta\text{-}CH_2}$	$a_{\gamma\text{-}CH_2}$	a_{2H}	a_{3H}	ref
4.86	4.7	4.7	1.0	<0.1	0.73	1.66	*b*
4.88	4.7	–	–	–	0.73	1.66	23[c]
4.81	4.7	–	–	–	0.76	1.65	24[c]

[a] At 298 K. Coupling constants in G. [b] This work for C_nTMB cation radicals. [c] For tetramethylbenzidine cation radical.

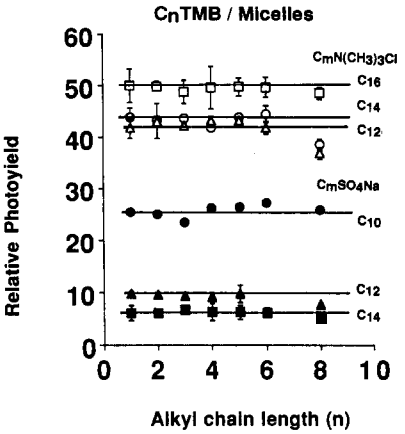

Figure 2. Relative photoyields of C_nTMB compounds versus the C_n alkyl chain length in anionic sodium alkyl sulfate micelles and in cationic alkyltrimethylammonium chloride micelles.

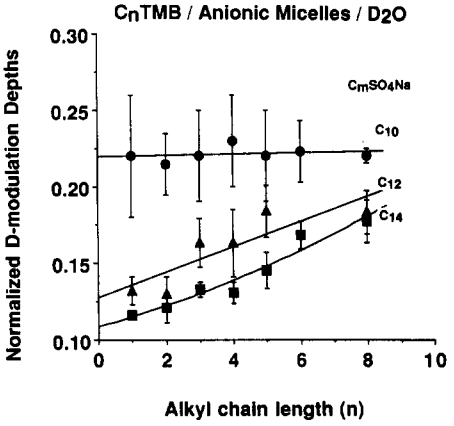

Figure 3. Normalized D-modulation depth from two-pulse ESEM at 4 K versus the C_n alkyl chain length in anionic sodium alkyl sulfate micelles.

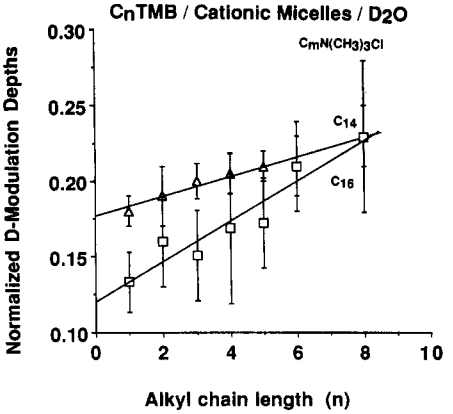

Figure 4. Normalized D-modulation depth from two-pulse ESEM at 4 K versus the C_n alkyl chain length in cationic alkyltrimethylammonium chloride micelles.

Changing the length of the surfactant monomer influences the size of the micelle. The longer the alkyl chain of the surfactant, the larger is the micelle. The surfactant chain length in cationic micelles has a negligible effect on the photoyield. The differences seen in the cationic micelles in Figure 2 are due primarily to the concentration of the electron donor used in each experiment; the

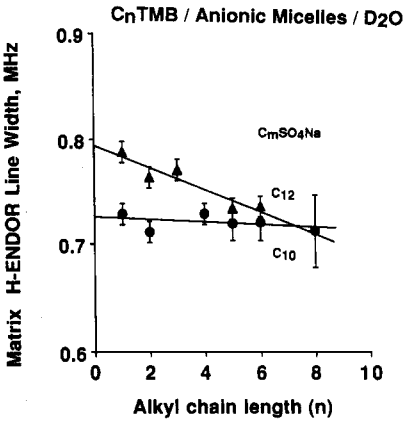

Figure 5. Proton matrix ENDOR line width versus the C_n alkyl chain length in anionic sodium alkyl sulfate micelles. The peak-to-peak derivative line width is given.

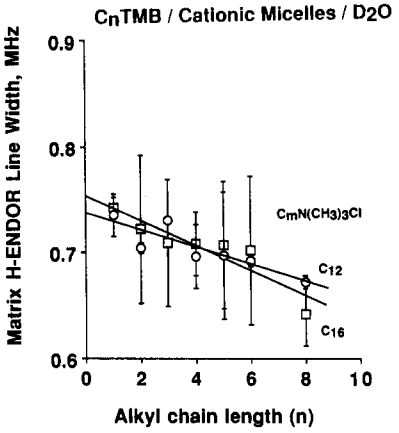

Figure 6. Proton matrix ENDOR line width versus the C_n alkyl chain length in cationic alkyltrimethylammonium chloride micelles. The peak-to-peak derivative line width is given.

$C_{16}N(CH_3)_3Cl$ micelles had more electron donor in solution than the other smaller micelles. Also, $C_{16}N(CH_3)_3Cl$ was 0.1 M in surfactant concentration while $C_{14}N(CH_3)_3Cl$ and $C_{12}N(CH_3)_3Cl$ were 0.2 M. In anionic micelles, the photoyield of C_nTMB^+ decreases monotonically as the surfactant chain length increases.

Secondary Radicals. The ESR spectrum in frozen cationic micelles is more complex than the signal that is produced in anionic micelles. The spectrum appears to consist of two radicals; the dominant signal is the benzidine cation radical singlet, and the other signal is a quartet with an intensity pattern 1:3:3:1 with a hyperfine coupling of about 23 G and a *g*-factor of approximately 2.002. This signal is identified as a methyl radical. The benzidine singlet comprises more than 95% of the total doubly integrated intensity. This was determined by subtracting a singlet signal generated in an anionic micelle of known doubly integrated intensity and scaling it appropriately to remove the singlet component in the cationic signal. When the methyl radical signal had as flat a baseline as possible, then the singlet component was judged to be accurately determined. In both cationic and anionic micelles, another radical in very low yield (<1%) is also found which has a spectral extent of more than 100 G. It is suspected to be an alkyl radical from the surfactant; this type of radical has been noted in both vesicles[26] and micelles.[25]

Initial Rate of Cation Radical Production. The data for the initial rate of C_nTMB cation radical production were analyzed by doubly integrating the ESR spectra and plotting it versus irradiation time. The initial slope of the photoyield curve shows no alkyl chain length effect on the initial rate of C_nTMB^+. The initial rate of cation radical production is constant within experimental error. The uncertainty in the initial rate of radical cation production is about 20%.

Discussion

ESEM and matrix ENDOR are two different techniques which give information about the nuclear environment in the immediate vicinity of a free radical. ESEM is a time domain and ENDOR is a double-resonance ESR technique. Both ESEM and ENDOR have been reviewed in the literature.[27-29] ESEM and ENDOR are complementary in that they give the same kind of information, but for different types of nuclei in the local environment.

A contrast in the nuclear environment is obtained when hydrocarbon surfactants with protons in natural abundance are dissolved in D_2O to form micelles. The interior of the micelle is proton rich and the aqueous phase deuteron rich. Thus, the ESEM-normalized deuterium modulation depth and the proton matrix ENDOR line width are altered when an organic free radical occupies a different solubilization location within the micelle. Both techniques are able to detect weak electron–nuclear interactions in frozen solids. Since the interaction is dipolar in nature, it is short ranged; at X-band, ESEM probes a spherical volume of about 0.6 nm[30] in radius while proton matrix ENDOR probes a slightly larger range of about 0.6–1.0 nm in radius (0.6, ref 31; 1.0, ref 32).

In both these techniques, it is the spin density over the entire free radical that interacts with the distribution of nearby nuclei. A question of the added alkyl chain's influence on the spin density of the benzidine radical arises. The solution-state ESR simulation indicates that the spin density on the β-carbon atom is small, and past the β-carbon it is negligible on an alkyl chain. A comparison of the deuterium ESEM and proton matrix ENDOR of C_1TMB and other C_nTMB compounds for $n \geq 2$ is valid since the bulk of the spin density remains on the nitrogens and α-carbons on the benzidine part of the molecule.

The ESEM nuclear modulation depth in the spin echo decay curve is proportional to the number of interacting nuclei and inversely proportional to the average distance to the nearby nuclear distribution. ESEM is also sensitive to the nuclear spin; the modulation depth intensity in the limit of small quadrupolar interaction is proportional to $I(I+1)$, where I is the nuclear spin quantum number. Thus, with the proton–deuteron contrast described above, ESEM can give a measure of the relative distance changes to the deuterated aqueous interface.

Proton matrix ENDOR lines occur at the nuclear Larmor frequency. The matrix ENDOR line arises due to purely dipole–dipole coupling between the unpaired electron and surrounding protons. A line shape analysis can yield some details about the surrounding magnetic nuclear environment. A model has been proposed that incorporates the distribution of protons around the radical with a relaxation mechanism formulated for dilute paramagnets in solids.[33] This model has given insights about the location of flavin radicals for flavoproteins[29] and recently has been applied to radicals solubilized in vesicles suspended in D_2O.[32] The matrix ENDOR line width of radicals solubilized in lipid membranes depends on the local proton density.[32] The local proton density is defined as the number of protons in a spherical shell in the immediate environment around the radical. The proton matrix ENDOR line width is broader for a larger number of nearby protons and vice versa. When there is a contrast in the magnetic nuclear environments as described above, then matrix ENDOR becomes a tool to determine changes in the location of a radical inside a lipid membrane.

Alkyl Chain Length Effect As Measured by ESEM and ENDOR. The degree of location control by changing the length of the added alkyl chain on an alkylbenzidine electron donor depends on the relative size of the micelle. In the largest anionic micelle examined here, the $C_{14}SO_4Na$ micelle, the ESEM shows an increasing normalized modulation depth and the matrix ENDOR shows a corresponding decrease in line width as the electron donor alkyl chain length increases. These two trends indicate that the benzidine moiety moves toward the aqueous interface of the micelle as the alkyl chain length increases. As the benzidine moiety moves toward the aqueous interface, the average distance from the center of this moiety and the water molecules (in this case D_2O) decreases, thus resulting in deeper deuteron modulation. Also, as the benzidine moiety moves toward the deuterated interface, the local proton density will decrease since more of the local spherical volume surrounding the radical will be occupied by interfacial D_2O. Consequently, the proton matrix ENDOR line becomes narrower.

However, in $C_{10}SO_4Na$ micelles, the smallest micelles investigated here, no location control as a function of added alkyl chain length is observed. The normalized deuterium modulation depth and proton matrix ENDOR line width are constant within experimental uncertainty. This is interpreted as no net movement of the benzidine moiety in the $C_{10}SO_4Na$ micelle as the alkylbenzidine chain length increases. The approximate length of an all-trans $C_{10}SO_4Na$ monomer is 1.2 nm, while the long axis of a neutral TMB molecule is also approximately 1.2 nm. One possibility is that in the relatively small $C_{10}SO_4Na$ micelle there is limited room for the benzidine moiety of an alkylbenzidine to move toward the interface as the alkylbenzidine chain length increases.

The same general trends for location control are shown for cationic micelles by adding alkyl chains of different lengths to the benzidine. Increasing the length of the alkyl chain moves the benzidine group toward the interface.

The size of the micelle also determines the magnitude of the water–radical interaction. This interaction in anionic micelles is seen to be a decreasing function of increasing surfactant alkyl chain length. This has been noted before for tetramethylbenzidine and alkylphenothiazines in both cationic and anionic micellar systems.[13,17] The fact that radicals solubilized in smaller micelles have a larger normalized modulation depth can be explained as simply being closer on average to the bulk and interfacial water for any given radical.

The normalized modulation depths of cationic micelles are larger than those for anionic micelles. This has been observed before[13,34] and is attributed to the higher hydration[34] at the surface of the cationic micelles compared to anionic micelles.

The qualitative trends of the ENDOR line width and the depth of the ESEM normalized modulation depth indicate the same changes in location of the photoproduced cation radical as a function of alkyl chain length. In general, the deuterium ESEM trends are expected to predict the trend of the proton matrix ENDOR line width and vice versa. When the ENDOR line width remains constant as a function of alkyl chain length in $C_{10}SO_4Na$, the normalized modulation depth is also constant. Also, as the normalized modulation depth increases as a function of the alkyl chain length in $C_{12}SO_4Na$, the ENDOR line width decreases.

Explanation of the Null Alkyl Chain Length Effect on the Photoyield in Micellar Alkylbenzidines. Why is there no change in the net photoyield as a function of alkyl chain length? In the larger micelles, ESEM and ENDOR show movement of the benzidine moiety toward the aqueous interface. Yet this increased water–donor contact does not translate into any increase of the photoyield as expected based on analogous systems.[4] For example, the *N*-alkylphenothiazines show an alkyl chain length effect on both the photoyield and the ESEM observed in cationic and anionic

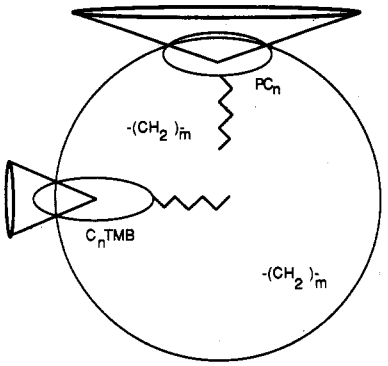

Figure 7. Schematic cross section of a spherical micelle with solubilized C_nTMB and N-alkylphenothiazine (PC_n). The electron escape cone is drawn from the center of the benzidine or phenothiazine moiety through the micellar interface intersecting the moiety. The C_nTMB is proposed to solubilize with its long axis along a micellar radial line, while the phenothiazine moiety is solubilized with its long axis perpendicular to a micellar radial line.

micelles.[13] The alkylbenzidines and N-alkylphenothiazines both show that the electron donor moiety moves toward the interface as the alkyl chain gets longer. Yet the magnitude and the relative change as a function of alkyl chain length in the normalized modulation depth are almost always larger in micelles with N-alkylphenothiazines.

These differences may be related to the geometry of solubilization of the electron donor moiety in the micelle. TMB has been proposed to solubilize with its long axis parallel to the long axes of the surfactant molecules to minimize micellar structure perturbation.[17] Electron spin echo data clearly indicate that TMB^+ is located in an asymmetric location within the micelle.[17] N-Alkylphenothiazines are suggested[13] to solubilize in a micelle with the long axis of the phenothiazine moiety perpendicular to a micellar radial line. Deuteron modulation depth magnitudes suggest that the alkylbenzidines solubilize deeper in micelles than do the alkylphenothiazines. This seems consistent with the different solubilization geometry proposed. Adding an alkyl chain to the benzidine moiety does not alter its solubilization geometry in a micelle.

To observe cation radicals generated by photoionization of electron donors in micelles, the photoproduced electron must escape the micelle and be ejected into the aqueous phase. There it is rapidly solvated, and it ultimately reacts with water to form H_2. In frozen polycrystalline aqueous micelles, no free electrons are observed by ESR. In micelles, the charge separation event may be thought to proceed through two steps; first the electron must tunnel through the hydrocarbon environment, and then it must penetrate an electrostatic interface. There are two possibilities at the interface depending on the charge of the surfactant head group. Anionic micelles form a barrier to be surmounted by the electron, while cationic micelles assist the passage of the photoejected electrons into the aqueous phase.[4] The details of electron tunneling in microheterogeneous media have been discussed, and the attenuation or "damping" factor of electron-tunneling transmission through hydrocarbon media has been briefly reviewed.[2] This damping factor is estimated to be on the order of 1–2 $Å^{-1}$. Thus, it may be concluded that the paths for most probable electron escape are those through the nearest surface with respect to the electron donor.[17,34] The most probable escape paths are affected by the solubilization geometry of an electron donor in a micelle. The paths for most probable escape form a cone from the center of the electron donor moiety through the width of the spin distribution that intersects the interface. Figure 7 shows that this electron escape cone increases faster as a function of alkyl chain length for alkylphenothiazines than it does for alkylbenzidines for the solubilization geometries shown. With more paths to generate charge-separated products, the photoyield is expected to be enhanced over that of an electron donor with a smaller solid angle of electron escape.

The rate at which the electron escape cone opens as a function of radial position in a micelle depends on the solubilization geometry. From Figure 7, it can be seen that for C_nTMB the escape cone grows slowly as a function of the radial position in the micelle. A simple analytic geometrical model where the benzidine moiety is an ellipse (major axis = 1.2 nm and minor axis = 0.5 nm) that intersects with a micellar interface of 2.0 nm in radius gives the angle of the electron escape cone as a function of the radial position in the micelle. For alkylbenzidine, the rate at which the cone opens as a function of radial position is 2°/nm. To model the alkylphenothiazine system, the major and minor axes are reversed compared to alkylbenzidine. For alkylphenothiazine, the cone opens more rapidly with an initial rate of cone opening of 31°/nm which drops to a rate of 3.2°/nm. This model calculation supports the assertion that the electron escape cone opens faster for alkylphenothiazines than it does for alkylbenzidines.

The initial slope of the radical cation yield versus time depends on several factors, including irradiating light intensity, initial electron donor concentration, the micelle size, and the micelle charge. Holding these factors constant should show any effect of electron donor solubilization location on the initial rate of cation radical production. The initial rate at which the benzidine cation radicals are formed is expected to be dependent on the aperture of the electron escape cone. For a wider escape cone, the rate of cation radical production should be faster than for a narrower escape cone. Yet the initial rate of radical cation production is independent of the alkylbenzidine chain length. This further supports the negligible change in electron escape aperture as a function of the alkylbenzidine chain length.

Conclusions

No alkyl chain length effect on the relative photoyield for long irradiation times as measured by CW-ESR is observed for N-alkyl-N,N',N'-trimethylbenzidines in ionic micelles. Deuterium ESEM and proton matrix ENDOR indicate that the solubilization location is altered by the alkyl chain length. C_nTMB compounds with shorter alkyl chains are solubilized more deeply in the micelle. As the added alkyl chain length increases, the benzidine moiety moves toward the aqueous interface, as evidenced by an increase in deuterium-normalized modulation depth and a decrease in the proton matrix ENDOR line width. However, the null effect of the alkyl chain length on the photoyield is counter to the observation that closer electron donor contact with the aqueous interface usually enhances the net photoyield. This suggests that the solubilization geometry implied by the structure of N-alkyl-N,N',N'-trimethylbenzidines compared to that of N-alkylphenothiazines is an important factor for net charge separation in micelles. The solubilization geometry determines the paths of most probable electron escape out of the micelle to form charge-separated products. These paths may be imagined as forming a solid angle from the center of the electron-donor moiety through the spin density of the molecule that intersects the aqueous interface. ESR evidence on the initial rate of benzidine cation radical production suggests that the electron escape cone is not alkyl chain length dependent, consistent with the geometric model proposed in Figure 7.

Acknowledgment. This research was supported by the Division of Chemical Sciences, Office of Basic Energy Sciences, Office of Energy Research, U.S. Department of Energy.

References and Notes

(1) Fendler, J. H.; Fendler, E. J. *Catalysis in Micellar and Macromolecular Systems*; Acedemic: New York, 1975; Chapter 8.
(2) Gratzel, M. *Heterogeneous Photochemical Electron Transfer*; CRC: Boca Raton, 1988.

(3) *Photochemical Conversion and Storage of Solar Energy*; Connolly, J. S., Ed.; Academic: New York, 1981.
(4) Kevan, L. *Int. Rev. Phys. Chem.* **1990**, *9*, 307–328.
(5) Maldonado, R.; Kevan, L.; Szajdzinska-Pietek, E.; Jones, R. R. M. *J. Chem. Phys.* **1984**, *81*, 3958–3961.
(6) Rivara-Minten, E.; Baglioni, P.; Kevan, L. *J. Phys. Chem.* **1988**, *92*, 2613–2615.
(7) Szajdzinska-Pietek, E.; Maldonado, R.; Kevan, L.; Jones, R. R. M. *J. Am. Chem. Soc.* **1985**, *107*, 6467–6470.
(8) Stenland, C.; Kevan, L. *Radiat. Phys. Chem.* **1991**, *37*, 423–426.
(9) Colaneri, M. J.; Kevan, L.; Schmehl, R. *J. Phys. Chem.* **1989**, *93*, 397–401.
(10) Baglioni, P.; Hu, M.; Kevan, L. *J. Phys. Chem.* **1990**, *94*, 2586–2590.
(11) Nakamura, H.; Baglioni, P.; Kevan, L.; Matsuo, T. *J. Phys. Chem.* **1991**, *95*, 1480–1484.
(12) Sakaguchi, M.; Kevan, L. *J. Phys. Chem.* **1991**, *95*, 5996–6000.
(13) Kang, Y. S.; Baglioni, P.; McManus, H. J. D.; Kevan, L. *J. Phys. Chem.* **1991**, *95*, 7944–7947.
(14) Alkaitis, S. A.; Gratzel, M. *J. Am. Chem. Soc.* **1976**, *98*, 3549–3554.
(15) Beck, S. M.; Brus, L. E. *J. Am. Chem. Soc.* **1983**, *105*, 1106–1111.
(16) Hashimoto, S.; Thomas, J. K. *J. Phys. Chem.* **1984**, *88*, 4044–4049.
(17) Narayana, P. A.; Li, A. S. W.; Kevan, L. *J. Am. Chem. Soc.* **1982**, *104*, 6502–6505.
(18) Ohta, N.; Kevan, K. *J. Phys. Chem.* **1985**, *89*, 2415–2419.
(19) Bernas, A.; Grand, D.; Hautecloque, S.; Giannotti, C. *J. Phys. Chem.* **1986**, *90*, 6189–6194.
(20) Grand, D.; Hautecloque, S. *J. Phys. Chem.* **1990**, *94*, 837–841.
(21) Imaizumi, H.; Sekiguchi, S.; Matsui, K. *Bull. Chem. Soc. Jpn.* **1977**, *50*, 948–952.
(22) Li, A. S. W.; Kevan, L. *J. Am. Chem. Soc.* **1983**, *105*, 5752–575.
(23) Smejtek, P.; Honzl, J.; Metalova, V. *Collect. Czech. Chem. Commun.* **1965**, *30*, 3875–3889.
(24) Horsman, G. In *Magnetic Resonance and Relaxation*, Proceedings of the XIVth Colloque Ampere; Blinc, R., Ed.; North Holland: Amsterdam, 1967; pp 578–585.
(25) Colaneri, M. J.; Kevan, L.; Thompson, D. H. P.; Hurst, J. K. *J. Phys. Chem.* **1987**, *91*, 4072–4077.
(26) Sakaguchi, M.; Kevan, L. *J. Phys. Chem.* **1989**, *93*, 6039–6043.
(27) Kevan, L. In *Radiation Research*, Proc. Seventh Intl. Congress; Broerse, J. J., Barendsen, G. W., Kal, H. B., Van der Kogel, A. J., Eds.; Martinus Nijhoff: Amsterdam, 1983; pp A5–O5.
(28) Kevan, L.; Kispert, L. D. *Electron Spin Double Resonance Spectroscopy*; Wiley: New York, 1976.
(29) Kevan, L. In *Photoinduced Electron Transfer Part B: Experimental Techniques and Medium Effects*; Fox, M. A., Chanon, M., Eds.; Elsevier: Amsterdam, 1988; pp 329–384.
(30) Kevan, L. In *Time Domain Electron Spin Resonance*; Kevan, L., Schwartz, R. N., Eds.; Wiley: New York, 1979; pp 279–341.
(31) Ehrenburg, A.; Eriksson, L. E. G.; Hyde, J. S. *Biochim. Biophys. Acta.* **1968**, *167*, 482–487.
(32) McManus, H. J. D.; Kevan, L. *J. Phys. Chem.* **1991**, *95*, 10172–10178.
(33) Hyde, J. S.; Rist, G. H.; Eriksson, L. E. G. *J. Phys. Chem.* **1968**, *72*, 4269.
(34) Baglioni, P.; Rivara-Minten, E.; Stenland, C.; Kevan, L. *J. Phys. Chem.* **1991**, *95*, 10169–10172.